Measurement of the electron cyclotron energy component of the electron beam of an electron beam ion trap

Peter Beiersdorfer[1] and Michelle Slater[1,2,*]
[1]*Department of Physics and Advanced Technologies, Lawrence Livermore National Laboratory, Livermore, California 94551*
[2]*Spelman College, Atlanta, Georgia 30314*
(Received 31 July 2001; published 26 November 2001)

The energy component associated with the cyclotron motion of the beam electrons in the Livermore EBIT-II electron beam ion trap was inferred from measurements of the linear polarization of the *K*-shell x-ray lines emitted from heliumlike Mg^{10+} ions. The average line polarization was found to be reduced by about 20% from its nominal value. From this it was inferred that the electron cyclotron motion accounted for 190 ± 30 eV of the total electron beam energy. The measured value is in good agreement with the predictions of optical electron beam propagation. It does not agree with the estimates derived from other model assumptions, such as the rigid-rotator model, for determining the size of the energy stored in the electron motion perpendicular to the beam propagation direction.

DOI: 10.1103/PhysRevE.64.066408 PACS number(s): 52.59.Sa, 52.70.La, 32.30.Rj

I. INTRODUCTION

The electron beam ion trap utilizes a magnetically compressed electron beam to produce, trap, and study essentially any ion from any element of choice [1–3]. Radial slots allow direct, line-of-sight access to the interaction region between the trapped ions and the electron beam. By measuring the radiation produced by the ions excited by the electron beam, cross section determinations for a variety of atomic processes have been possible. Examples are measurements of excitation [4–7], ionization [8,9], and dielectronic recombination [10–15] cross sections.

The use of an electron beam interacting with quasistationary ions means that the emitted radiation generally is both anisotropic and polarized [16,17]. As a result, the intensity of a given emission feature from a beam-excited ion depends on the observation angle relative to the axis defined by the electron beam. It also depends on whether or not the emission is analyzed with polarization-sensitive instrumentation. In some regards, these phenomena are similar to those encountered in beam-foil spectroscopy [18], where a beam of ions traverses a cloud of electrons ''trapped'' in a foil. In both cases, adjustments to account for polarization effects must be made lest wrong results are obtained.

Adjustments for polarization effects in electron beam ion trap experiments are not without complications. One reason is that a given electron in the electron beam does not simply travel in the direction of beam propagation. Its path instead traces out a helix, as it spirals around the magnetic field lines aligned with the beam propagation axis. Ions, therefore, interact with electrons with velocity vectors that deviate from that of the beam direction. The net result is that the amount of polarization is reduced from what it would be, if all electrons were truly following a straight line along the magnetic field direction.

The amount of depolarization depends on the pitch angle of the electron motion, i.e., on the angle γ between the magnetic field line and electron's velocity vector. This angle is determined by the ratio of the electron's velocity component along the magnetic field line and that perpendicular,

$$\tan\gamma = \frac{v_\perp}{v_\parallel}, \tag{1}$$

or

$$\sin\gamma^2 = \frac{E_\perp}{E_{beam}}, \tag{2}$$

where E_{beam} is the beam energy and $E_\perp$ is the electron energy in the motion perpendicular to the beam propagation direction. A simple expression that describes the reduction in the polarization of the emitted radiation as a function of the pitch angle was recently derived by Gu, Savin, and Beiersdorfer [19]. For electric dipole radiation they showed that the polarization P is reduced to

$$P = P_0 \frac{2 - 3\sin\gamma^2}{2 - \sin\gamma^2 P_0}. \tag{3}$$

Here P_0 is the polarization for a zero pitch angle.

The perpendicular velocity component can be estimated from several considerations. Beiersdorfer *et al.* used the Herrmann theory of optical electron beam propagation to estimate 110 eV for the value of $E_\perp$ in Livermore's EBIT-II electron beam ion trap [20]. Independently, Takács *et al.* estimated a value of 700 eV for the National Institute of Standards and Technology (NIST) electron beam ion trap using the theory of rigid beam rotation [21]. They estimated an even higher value ($\leqslant 1000$ eV) based on the principle of adiabatic magnetic flux invariance.

The nearly one-order-of-magnitude difference in the estimated energy stored in the electron motion perpendicular to the beam propagation direction estimated by the two groups is disconcerting in the light of the fact that this estimate is a critical parameter used to adjust the values of the observed radiation and thus, for example, of measured electron-ion interaction cross sections.

*Deceased

Takács *et al.* supported their choice of methods for estimating the perpendicular energy component by pointing to the fact that the NIST electron beam ion trap can be operated only as low as 700 eV [21]. Their suggestion is that at this energy all electron energy is in the perpendicular motion so that beam propagation no longer takes place. This result is surprising given that the NIST electron beam ion trap was build according to the Livermore design [22], — and both Livermore devices, EBIT-II and SuperEBIT, can be operated with a beam energy as low as 100 eV [23,24]. By the same reasoning, the optical theory of beam propagation should be the correct model, as only it predicts perpendicular energies as low as 100 eV. While it is true that the NIST electron beam ion trap is not a complete copy of the Livermore design—some small design changes were made that were intended to improve the performance of its operation [22], the design differences are not sufficient to mandate a choice of model for estimating $E_\perp$ that differs for the three devices. In fact, the design difference between the two Livermore electron beam ion traps is by far much larger than between EBIT-II and the NIST electron beam ion trap.

The large spread in estimates clearly make a measurement of the perpendicular energy component highly desirable in order to discriminate among the models. In the following we employ the techniques of plasma polarization spectroscopy for determining $E_\perp$. Plasma polarization spectroscopy has already been applied to tokamak, solar, and laser-produced plasmas for determining nonequilibrium components of the electron distribution function [25–27]. Our measurement favors the prediction based on the Herrmann theory of optical electron beam propagation, giving a value of 190 ± 30 eV for $E_\perp$.

II. EXPERIMENT

The measurement is carried out on the EBIT-II electron beam ion trap using the vacuum flat-crystal spectrometer described in Ref. [28]. The instrument is mounted on one of six ports viewing the ions in the trap in the direction perpendicular to the beam. The plane of dispersion is parallel to the plane perpendicular to the beam direction, as illustrated in Fig. 1. The opening angle of the detector in the vertical direction is less than 0.8°. This is sufficiently small as to provide a reliable sample of radiation emitted at 90° to the beam propagation direction.

The spectrometer utilizes a thallium-acid-phtalate crystal (TlAP) with a lattice spacing $2d=25.76$ Å. This crystal is well suited to record the *K*-shell x-ray lines of heliumlike Mg^{10+} and study the effect of polarization. The Mg^{10+} spectrum is centered around 9.25 Å. In first order Bragg reflection, the observation angle is 21.4°. In second order, the observation angle is 45.2°. In the latter position, only the emission component with electric field vector parallel to the plane of the crystal (and parallel to the electron beam propagation) is reflected and counted. In the former position, a mixture of both polarization components are reflected and counted. The present measurement utilizes the differences in the crystal response at these two Bragg angles to determine the polarization of the observed lines. The present method is similar to the two-crystal method employed in earlier measurements on the EBIT-II and SuperEBIT electron beam ion traps [20,29–32].

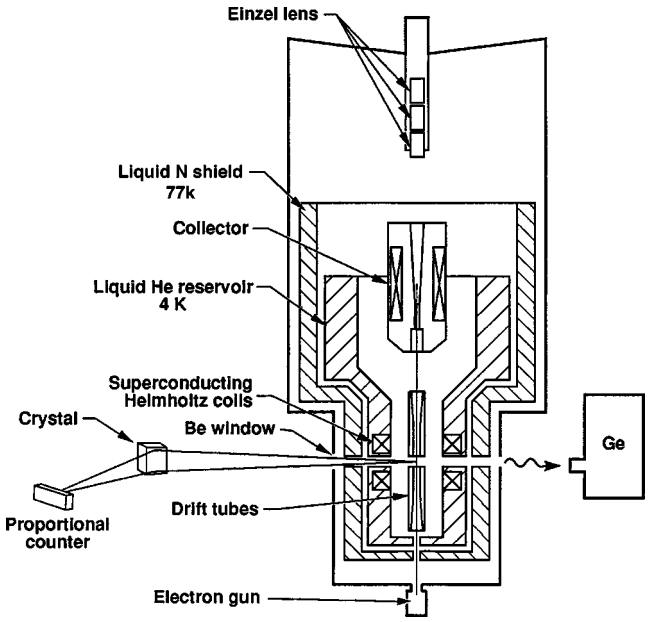

FIG. 1. Layout of the flat-crystal spectrometer on the EBIT-II electron beam in trap. Ions are produced and trapped in a 2-cm-long region between the superconducting Helmholtz coils. The ions are excited by an electron beam propagating between the electron gun and the collector. X rays are monitored via the radial ports in the vacuum vessel and are analyzed and dispersed with the crystal spectrometer in the plane perpendicular to the propagation direction of the electron beam.

The observed Mg^{10+} spectrum is comprised of the $1s2p\ ^1P_1\rightarrow1s^2\ ^1S_0$ resonance line, the blend of the $1s2p\ ^3P_1\rightarrow1s^2\ ^1S_0$ intercombination line and the $1s2p\ ^3P_2\rightarrow1s^2\ ^1S_0$ magnetic quadrupole line, and the $1s2s\ ^3S_1\rightarrow1s^2\ ^1S_0$ forbidden line, which are commonly labeled w, y, x, and z, respectively.

We have chosen the lines in heliumlike magnesium for determining the amount of depolarization because the polarization P_0 of these lines in the absence of depolarization effects is well known from theory and experiment. The polarization of lines w and x is within a few percent the same for all low- and mid-Z heliumlike ions at similar electron-collision energies expressed in threshold units [33,34]. Within a few percent above excitation threshold the polarization of w and x is $P_0(w)=0.60$ and $P_0(x)=-0.52$, respectively. The accuracy of these calculations have been experimentally verified for several heliumlike ions [20,32,35].

The value of the polarization of x determines the value of the polarization of z. In magnesium, the $1s2p\ ^3P_2$ upper level of x decays 93% of the time to the $1s2s\ ^3S_1$ upper level of z. Following the expression derived in Ref. [20], the polarization $P_0(z)$ of z in terms of the polarization $P_0(x)$ of x is

$$P_0(z)=+\frac{3kP_0(x)}{3\sqrt{5/7}-P_0(x)(\sqrt{5/7}+k)}. \qquad (4)$$

The factor k is proportional to the fractional excitation of z by cascades from the $1s2p\,^3P_2$ level [20]. It was shown in Ref. [32] to depend only on the branching ratio β_r for radiative decay of the $1s2p\,^3P_2$ level to the $1s2s\,^3S_1$ level. For $\beta_r = 0.93$ [36] we find $k = 0.377$.

Another reason to pick heliumlike magnesium for determining the amount of depolarization is that the atomic number of magnesium is low enough so that LS coupling is valid. This eliminates the uncertainty in ascertaining the polarization of line y, as the $1s2p\,^3P_1$ upper level of y mixes only negligibly with the $1s2p\,^1P_1$ upper lever of w. The polarization of y, therefore, equals that of x, and the unresolved blend of y and x has the same polarization as x or y alone.

The spectrum of the magnesium Kα transitions recorded with the TlAP crystal in first order is shown in Fig. 2(a). The spectrum recorded in second order is shown in Fig. 2(b). The second order spectrum has considerably higher resolution than the first order spectrum. This is expected from the higher intrinsic resolving power of the crystal in second order Bragg reflection and the fact that the resolving power increases with the tangent of the Bragg angle. The data were accumulated at a beam energy that was about 50 eV above threshold for direct excitation of the lines of interest, avoiding the above-threshold KMM resonances.

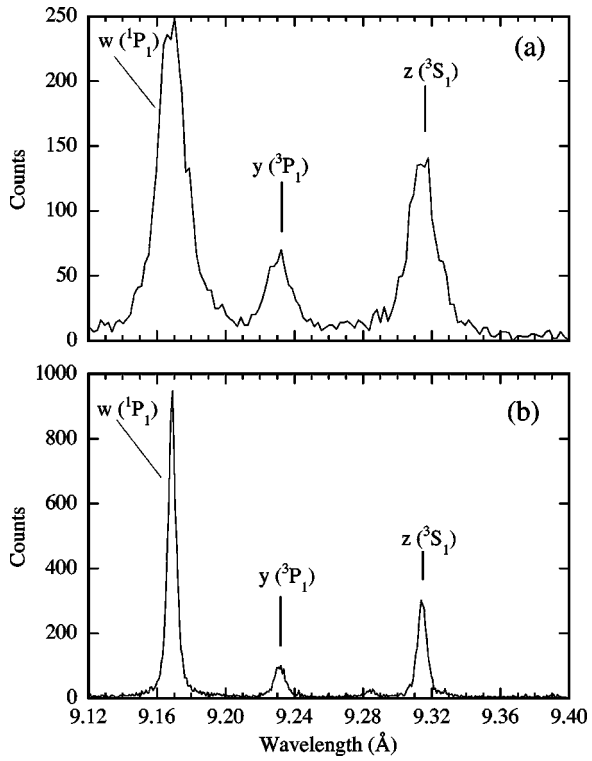

FIG. 2. Crystal-spectrometer spectra of lines w, x, y, and z in Mg^{10+} excited by a 1400 eV electron beam. (a) spectrum obtained with a TlAP crystal in first order reflection at a Bragg angle of 21°; (b) spectrum obtained with the same crystal in second order reflection at a Bragg angle of 45°.

III. ANALYSIS

The relative intensities of the heliumlike lines shown in Fig. 2 are clearly different in the two spectra. To obtain a quantitative measure of the intensity of each feature we used least-squares fits of different trial functions to the line: a single Gaussian, a double Gaussian, a Lorenztian, and a mixture of a Lorentzian and a Gaussian trial function. The double trial functions are used to fit the rather narrow peak and the rather wide base of the observed lines. The intensities determined from the fits with these trial functions are listed in Table I.

The fits with the double trial functions gave much better fits then those with a single function. The use of a Lorenztian function (either alone or in combination with a Gaussian) was somewhat problematic, because the inherently broad tails are poorly constrained and may readily lead to spurious results. This is true even if the residuals intimate an excellent fit. Because of their extensive tails, the fits involving a Lorentzian function result in considerably higher line intensities than using only Gaussian functions.

The intensities in Table I are used to infer the polarization of a given line relative to the polarization of second line. As shown in Ref. [32], we can express the polarization P_a of line a in terms of the polarization P_b of line b,

$$P_a = \frac{\left.\frac{I^a}{I^b}\right|_1 \left(1 + R_1 \frac{1-P_b}{1+P_b}\right)(R_2+1) - \left.\frac{I^a}{I^b}\right|_2 \left(1 + R_2 \frac{1-P_b}{1+P_b}\right)(R_1+1)}{\left.\frac{I^a}{I^b}\right|_1 \left(1 + R_1 \frac{1-P_b}{1+P_b}\right)(R_2-1) - \left.\frac{I^a}{I^b}\right|_2 \left(1 + R_2 \frac{1-P_b}{1+P_b}\right)(R_1-1)}. \tag{5}$$

Here I^a/I^b is the intensity ratio of lines a and b. The subscripts refer to the order of Bragg reflection in which the ratio is measured. $R = R_\perp / R_\parallel$ is the ratio of the integrated crystal reflectivities for x rays polarized perpendicular and parallel to the electron beam directions, i.e., parallel and perpendicular to the plane of dispersion, respectively. Again, the subscripts refer to the order of Bragg reflection. The values of R are taken from [37]: $R_1 = 0.605$ and $R_2 = 0.004$.

Using the iterative procedure described in Ref. [32] and the fact that the polarization of z is completely determined by the polarization of x (and thus of y), we can determine the polarizations of all lines from the data in Table I. The results

TABLE I. Intensities of the heliumlike lines w, $x+y$, and z measured in first and second order with a TlAP crystal obtained with different trail functions.

	Single Gaussian		Double Gaussian		Lorentzian+Gaussian		Single Lorenztian	
Line	1st	2nd	1st	2nd	1st	2nd	1st	2nd
w	2750	7672	2820	7814	3137	8331	3168	8586
$x+y$	708	1066	707	991	679	1078	679	1168
z	1487	2724	1567	2830	1720	3069	1761	3230

are given in Table II.

The polarization values inferred from the four different fitting procedures show interesting trends. The inferred polarization of w increases from $P=0.46$ to $P=0.64$ when considering the single and double Gaussian fits, the Gauss-Lorentzian fit, and the single Lorentzian fit. The value inferred from the Lorentzian fit is larger than that predicted by theory, and thus is unphysically large. Similarly, the inferred polarizations of the blend of the intercombination lines x and y steadily increase from $P=-0.40$ inferred from the single-Gaussian fit to $P=-0.13$ inferred from the single Lorentzian fit. The inferred polarizations of the forbidden line z steadily increase from $P=-0.15$ to $P=-0.055$. The result is that the fits involving a Lorentzian function show a strong depolarization of lines x, y, and z, while they show that line w experiences no depolarization or even an increase in its polarization value. The results inferred from fits involving Lorenztian functions are, thus, highly contradictory. By contrast, the polarization values derived from fitting Gaussian functions to the data are self-consistent. All three line features show similar amounts of depolarization.

By comparing the polarization values inferred from the line intensities in Table I to those predicted by theory (listed in the last column of Table II), we can determine the amount of depolarization and thus $E_\perp$. Solving Eq. (3) for $E_\perp$, we get

$$E_\perp = \frac{2(P_0 - P_i)}{P_0(3-P_i)} E_{beam}, \tag{6}$$

where i refers to lines w, $x+y$, and z. The resulting values are listed in Table III.

The internal inconsistency of the data inferred from the Lorentzian fits is even better seen in when looking at the $E_\perp$ values listed in Table III: The $E_\perp$ values derived for w range from a nonphysical -35 eV to $+4$ eV; those derived for the other features range from $+931$ to $+1920$ eV. These inconsistencies arise from the poor constraint on the wide wings afforded by the Lorentzian trial function.

By contrast the Gaussian fits give $E_\perp$ values that range from 100 to 277 eV for w, and from 154 to 229 eV for the three triplet lines. The results are plotted in Fig. 3. These results are clearly consistent with each other. In fact, the results strongly suggest that a fitting function might exist for which all three features yield the same value of $E_\perp$. The average value of $E_\perp$ is 190 ± 30 eV.

TABLE II. Polarization inferred from the data in Table I. Also listed are the polarization values for an electron beam without a perpendicular component of electron motion.

Line	Single Gaussian	Double Gaussian	Lorentzian +Gaussian	Single Lorenztian	Theory
w	0.46	0.55	0.61	0.64	0.614
$x+y$	-0.40	-0.37	-0.205	-0.13	-0.519
z	-0.15	-0.14	-0.083	-0.055	-0.185

IV. DISCUSSION

Our result of $E_\perp = 190\pm30$ eV is in agreement with the predictions of the optical approach by Herrmann [38]. Herrmann showed that cathode images are formed at various locations along the beam axis, whereby the magnitude of the transverse velocity is inversely proportional to the radii of the images. This means that the product of beam area and tranverse electron energy $E_\perp$ is a constant. $E_\perp$ can thus be estimated from the temperature of the cathode of the electron gun and the areal compression ratio of the beam. The gun temperature is about 1400 K (0.123 eV), and the beam radius at the cathode is about 1 mm. The beam is compressed to about 25 μm in the trap. Using these values, we obtain $E_\perp = 194$ eV, in full agreement with our measurements. These values, however, are only estimates; they are not well known. But the answer shows that consistency with our measurements can readily be achieved. The temperature of the filament may vary between 1000 to 1600 K, depending on the filament heating current. Similarly, the radius of the electron beam may vary between 25 to 35 μm, depending on such parameters as the beam current and bucking coil setting. As a result, the value of $E_\perp$ predicted by the Herrmann theory may vary between 50 to 250 eV. The estimate of 110 eV provided in Ref. [20] falls well within this range.

Our measured value does not agree with the 700 eV prediction provided by the rigid rotator approach employed by Takács *et al.* to describe the electron beam ion trap at NIST

TABLE III. Values of $E_\perp$ inferred from the data in Table II.

Line	Single Gaussian (eV)	Double Gaussian (eV)	Lorentzian +Gaussian (eV)	Single Lorenztian (eV)
w	277	100	4	-35
$x+y$	165	229	956	1920
z	154	217	931	1880

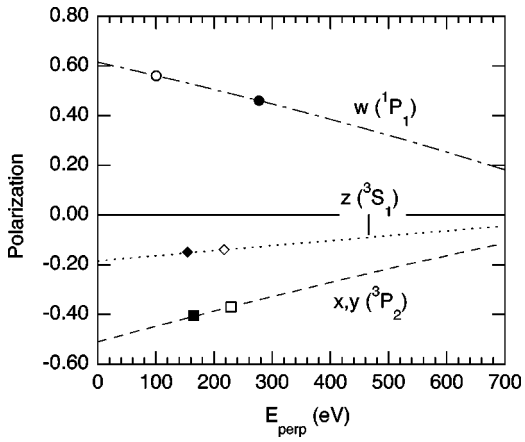

FIG. 3. Dependence of the linear x-ray polarization of lines *w*, *x*, *y*, and *z* of Mg^{10+} on the size of the electron energy component perpendicular to the beam propagation direction. The total beam energy is set to 1400 eV. Measured values are shown for spectral data analyzed with single Gaussian (solid symbols) and double Gaussian (open symbols) trial function fits.

[21]. The rigid rotator approach assumes a uniform electron density within a cylindrical volume [39]. Such an idealized situation is not realized in an electron beam ion trap. Not only are there gradients in the radial electron density, there are strong gradients along the electron beam direction. The magnetic field of the Helmholtz coils is uniform only throughout a relatively small length within the trap region (about 4 cm). The magnetic field, and thus the beam radius and electron density, are highly nonuniform for the remaining $\geqslant 95\%$ of the beam path. There is no reason why the rigid rotor model should be applicable, and our measurements bear this out. The strong magnetic field gradients (from essentially zero field at the gun to 30 000 gauss in the trap) that are traversed by fast moving electrons also invalidate the applicability of the principle of adiabatic magnetic flux invariance.

Our measurements provide strong support for the optical beam transport theory derived by Herrmann [38]. This is comforting, as the Herrmann theory was used as one of the underlying principles in the design of the electron beam ion trap [1]. The Herrmann theory yields a good upper bound of the energy in the electron cyclotron motion, and thus provides an upper bound on the amount of depolarization of the emitted radiation.

ACKNOWLEDGMENTS

This work was performed by the University of California Lawrence Livermore National Laboratory under the auspices of the Department of Energy under Contract No. W-7405-ENG-48. It was supported by the Office of Basic Energy Sciences, Division of Chemical Physics. Additional support from the Livermore Collaborations Program for Historically Black Colleges and Universities and Minority Institutions is gratefully acknowledged.

[1] M. A. Levine, R. E. Marrs, J. R. Henderson, D. A. Knapp, and M. B. Schneider, Phys. Scr. **T22**, 157 (1988).
[2] M. A. Levine, R. E. Marrs, J. N. Bardsley, P. Beiersdorfer, C. L. Bennett, M. H. Chen, T. Cowan, D. Dietrich, J. R. Henderson, D. A. Knapp, A. Osterheld, B. M. Penetrante, M. B. Schneider, and J. H. Scofield, Nucl. Instrum. Methods Phys. Res. B **43**, 431 (1989).
[3] R. E. Marrs, P. Beiersdorfer, and D. Schneider, Phys. Today **47**(10), 27 (1994).
[4] S. Chantrenne, P. Beiersdorfer, R. Cauble, and M. B. Schneider, Phys. Rev. Lett. **69**, 265 (1992).
[5] P. Beiersdorfer, in *Electron and Atomic Collisions – XVII ICPEAC, Brisbane, 1991*, edited by W. R. MacGillivray, I. E. McCarthy, and M. C. Standage (Adam Hilgar, Bristol, 1992), p. 313.
[6] K. L. Wong, P. Beiersdorfer, K. J. Reed, and D. A. Vogel, Phys. Rev. A **51**, 1214 (1995).
[7] M. F. Gu, S. M. Kahn, D. W. Savin, P. Beiersdorfer, G. V. Brown, D. A. Liedahl, K. J. Reed, C. P. Bhalla, and S. R. Grabbe, Astrophys. J. **518**, 1002 (1999).
[8] K. Wong, P. Beiersdorfer, M. H. Chen, R. E. Marrs, K. J. Reed, J. H. Scofield, D. A. Vogel, and R. Zasadzinski, Phys. Rev. A **48**, 2850 (1993).
[9] R. E. Marrs, S. R. Elliott, and J. H. Scofield, Phys. Rev. A **56**, 1338 (1997).
[10] P. Beiersdorfer, T. W. Phillips, K. L. Wong, R. E. Marrs, and D. A. Vogel, Phys. Rev. A **46**, 3812 (1992).
[11] P. Beiersdorfer, M. B. Schneider, M. Bitter, and S. von Goeler, Rev. Sci. Instrum. **63**, 5029 (1992).
[12] D. A. Knapp, R. E. Marrs, M. B. Schneider, M. H. Chen, M. A. Levine, and P. Lee, Phys. Rev. A **47**, 2039 (1993).
[13] A. J. Smith, P. Beiersdorfer, V. Decaux, K. Widmann, K. J. Reed, and M. H. Chen, Phys. Rev. A **54**, 462 (1996).
[14] A. J. Smith, P. Beiersdorfer, K. Widmann, M. H. Chen, and J. H. Scofield, Phys. Rev. A **62**, 052717 (2000).
[15] B. J. Wargelin, S. M. Kahn, and P. Beiersdorfer, Phys. Rev. A **63**, 022710 (2001).
[16] J. R. Oppenheimer, Z. Phys. **43**, 27 (1927).
[17] I. C. Percival and M. J. Seaton, Philos. Trans. R. Soc. London, Ser. A **251**, 113 (1958).
[18] H. G. Berry, L. J. Curtis, D. G. Ellis, and R. M. Schectman, Phys. Rev. Lett. **32**, 751 (1974).
[19] M.-F. Gu, D. W. Savin, and P. Beiersdorfer, J. Phys. B **32**, 5371 (1999).
[20] P. Beiersdorfer, D. A. Vogel, K. J. Reed, V. Decaux, J. H. Scofield, K. Widmann, G. Hölzer, E. Förster, O. Wehrhan, D. W. Savin, and L. Schweikhard, Phys. Rev. A **53**, 3974 (1996).
[21] E. Takács, E. S. Meyer, J. D. Gillaspy, J. R. Roberts, C. T. Chandler, L. T. Hudson, R. D. Deslattes, C. M. Brown, J. M. Laming, J. Dubau, and M. K. Inal, Phys. Rev. A **54**, 1342 (1996).
[22] J. D. Gillaspy, Phys. Scr. **T71**, 99 (1997).
[23] E. Träbert, P. Beiersdorfer, and S. B. Utter, Phys. Scr. **T80**, 450 (1999).

[24] P. Beiersdorfer, J. K. Lepson, G. V. Brown, S. B. Utter, S. M. Kahn, D. A. Liedahl, and C. W. Mauche, Astrophys. J. Lett. **519**, L185 (1999).
[25] T. Fujimoto, T. Kawachi, T. Kallstenius, M. Goto, H. Kawase, T. Furukubo, T. Maekawa, and Y. Terumichi, Phys. Rev. E **54**, R2240 (1996).
[26] E. Haug, Sol. Phys. **71**, 77 (1981).
[27] H. Yoneda, N. Hasegawa, S. Kawana, and K. Ueda, Phys. Rev. E **56**, 988 (1997).
[28] P. Beiersdorfer and B. J. Wargelin, Rev. Sci. Instrum. **65**, 13 (1994).
[29] P. Beiersdorfer, J. Crespo López-Urrutia, V. Decaux, K. Widmann, and P. Neill, Rev. Sci. Instrum. **68**, 1073 (1997).
[30] A. S. Shlyaptseva, R. C. Mancini, P. Neill, P. Beiersdorfer, J. Crespo López-Urrutia, and K. Widmann, Phys. Rev. A **57**, 888 (1998).
[31] A. S. Shlyaptseva, R. C. Mancini, P. Neill, and P. Beiersdorfer, J. Phys. B **32**, 1041 (1999).
[32] P. Beiersdorfer, G. Brown, S. Utter, P. Neill, K. J. Reed, A. J. Smith, and R. S. Thoe, Phys. Rev. A **60**, 4156 (1999).
[33] Y. Itikawa, R. Srivastava, and K. Sakimoto, Phys. Rev. A **44**, 7195 (1993).
[34] K. J. Reed and M. H. Chen, Phys. Rev. A **48**, 3644 (1993).
[35] J. R. Henderson, P. Beiersdorfer, C. L. Bennett, S. Chantrenne, D. A. Knapp, R. E. Marrs, M. B. Schneider, K. L. Wong, G. A. Doschek, J. F. Seely, C. M. Brown, R. E. LaVilla, J. Dubau, and M. A. Levine, Phys. Rev. Lett. **65**, 705 (1990).
[36] C. D. Lin, W. R. Johnson, and A. Dalgarno, Phys. Rev. A **15**, 154 (1977).
[37] B. L. Henke, E. M. Gullikson, and J. C. Davis, At. Data Nucl. Data Tables **54**, 181 (1993).
[38] G. Herrmann, J. Appl. Phys. **29**, 127 (1958).
[39] N. A. Krall and A. W. Trivelpiece, *Principles of Plasma Physics* (McGraw-Hill, New York, 1973), p. 117.